14.1 SCALAR FLUX PROFILE RELATIONSHIPS FOR WATER VAPOR OVER THE OPEN OCEAN

James Edson, Christopher Zappa, and Wade McGillis
Woods Hole Oceanographic Institution, Woods Hole, Massachusetts

1. INTRODUCTION

Over the ocean, direct measurement of turbulent air-sea fluxes are difficult due to platform motion, flow distortion, and the effects of sea-spray. Instead, flux-profile relationships that relate the turbulence fluxes of momentum, heat and moisture (or mass) to their respective profiles of velocity, temperature, and water vapor (or other gases) have been used. These flux-profile relationships are required in indirect methods such as the bulk aerodynamic, profile, and inertial dissipation methods that estimate the fluxes from mean, profile, and high frequency spectral measurements, respectively. The flux-profile or flux-gradient relationships are also used extensively in numerical models to provide lower boundary conditions and to "close" the model by approximating higher order terms from low order variables.

The most commonly used flux-profile relationships are based on Monin-Obukhov similarity theory. MO similarity has been validated by a number of overland experiments including the landmark Kansas, Minnesota, and ITCE experiments in the 1970s. These and other experiments have generated a number of similar semi-empirical functions that are used in the indirect methods over the ocean. However, the use of overland measure-ments to infer ocean surface fluxes has been questionable, particularly close to the ocean surface where wave-induced forcing can affect the flow. Therefore, the relationship universality to all surface layers is a current topic of research.

2. THE 2001 GASEX EXPERIMENT

The GasEx-2001 study took place in February 2001 in the Eastern Equatorial Pacific (3ºS 125ºW). The objective was to continue with recent progress using micrometeorological flux measurements to improve the understanding of the forcing functions on air-sea exchange, particularly of gases (McGillis et al., 2001). Direct measurement of the atmospheric fluxes along with profiles of water vapor and temperature were made during the 2001 GasEx experiment. The measurements were made from the NOAA R/V Ronald H. Brown at the end of a boom that placed the sensors 10-m upwind of the bow (Figure 1). Turbulent fluxes of momentum, heat, and water vapor were made by sonic anemometers, sonic thermometers and infrared hygrometers, respectively. A mast at the end of the 10-m boom supported a profiling system that moved a suite of sensors between 4 and 12 meters above the mean ocean surface. The moving sensors were referenced against a fixed suite of sensors to remove naturally occurring variability during the profiling periods.

Figure 1. The NOAA R/V Ronald H. Brown outfitted with a bow boom and mast for the February 2001 GasEx experiment performed at 3S and 125W.

Figure 2. The boom extended 10 m from the bow. The 8-m mast extended from 4-12 m above the ocean surface.

3. MONIN-OBUKHOV SIMILARITY THEORY

Monin-Obukhov (MO) similarity theory states that the structure of turbulence is determined by the height above the surface, z, the buoyancy term, g/Θ_v (Θ_v is the virtual potential temperature), the friction velocity, u_*, and the surface buoyancy flux, $\overline{w\theta_v}_s$. These last two terms are defined from the surface stress and heat fluxes as

* *Corresponding author address*: WHOI, J. Edson, MS #12, 98 Water Street, Woods Hole, MA, 02543; email: jedson@whoi.edu.

$$u_* = \left[\frac{|\vec{\tau}_a(0)|}{\rho_a}\right]^{1/2} \quad (1)$$

$$\overline{w\theta_{v_s}} = \frac{Q_h}{\rho_a c_p} + 0.61\, T_s \frac{Q_e}{\rho_a L_e} \quad (2)$$

where $\vec{\tau}_a(0)$ is the surface stress vector, Q_h is the surface value of the sensible heat flux, Q_e is the surface value of the latent heat flux, T_s is the surface temperature, c_p is the specific heat at constant pressure, ρ_a is the density of air, and L_e is the latent heat of vaporization of water.

The velocity scale, u_* is then used to define temperature and moisture scales

$$T_* = -\frac{\overline{w\theta_o}}{u_*} \quad , \quad \rho_{v_*} = -\frac{\overline{w\rho_{v_o}}}{u_*} \quad , \quad (3)$$

and MO length scale

$$L = -\frac{\Theta_v\, u_*^3}{g\kappa\, \overline{w\theta_{v_o}}} \quad , \quad (4)$$

where w, θ, and ρ_v denote vertical velocity, potential temperature, and water vapor fluctuations, respectively; the symbol o denotes surface values; the overbar denotes a time average; and κ is the von Karman constant. The height at which $z = L$ represents the height where mechanical and thermal forcing are of equal magnitude.

The similarity hypothesis then states that various turbulent statistics, when normalized by these scaling parameters, are a universal function of z/L. For example, normalization of the water vapor profile by $\rho_{v_*}/\kappa z$ is expected to collapsed to a universal function

$$\phi_q\left(\frac{z}{L}\right) = \frac{\kappa z}{\rho_{v_*}} \frac{\partial \overline{\rho_v}}{\partial z} \quad (5)$$

These scaling laws are expected to be universal as long as the assumptions that govern the similarity laws are valid (a combination of mechanical and thermal forcing drive the turbulent exchange, the scaling variables are independent of height in the surface layer, and the turbulence statistics are stationary and horizontally homogeneous). In the particular case of the marine surface layer, the former assumption can become invalid when wave induced flow plays an important role in turbulent exchange. This near surface region of the marine boundary layer is referred to as the wave boundary layer (WBL). The height defined as the top of the WBL varies with different models, but the WBL is generally thought to include the height where $kz < 1$ where k is the wavenumber of the dominant waves.

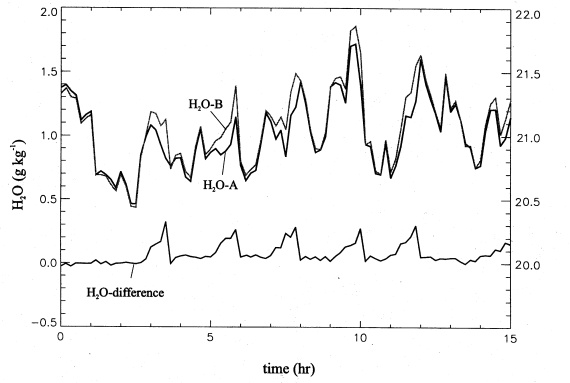

Figure 3: Time series of atmospheric water vapor concentration plotted as specific humidity from a fixed position (H2O-A) and from the profiler (H2O-B). The lower time series is the difference of the two measurements.

4. RESULTS

The water vapor profiles are generated using a single sensor that travels the extent of the mast located at the end of the bow boom. A single profile takes 1 hour to complete (4 levels at 15 minutes each). As shown in Figure 3, naturally occurring temporal variability in atmospheric water vapor generates differences over time that are often larger than the differences due to the gradient during this period, i.e., the temporal variability of water vapor (σ = 0.278 g kg^{-1}) is greater than the vertical boundary layer gradients (σ = 0.085 g kg^{-1}). However, we can remove most of the temporal variability by taking the difference between the profiling sensor and a fixed sensor at 8 m. The difference is shown by the lower time series in Figure 3 where the vertical gradient is now clearly visible. This approach also reduces the intercalibration problems that arise with fixed sensor arrays due to sensor drift and contamination.

To further reduce the uncertainty in our measurements, we removed profiles measured during rain events, when the relative wind direction was greater than 90^o from the bow, and when the ship changed course during a run. Additionally, we attempted to remove outliers by including only those profiles with $R^2 > 0.95$. This effectively removes profiles that do not monotonically decrease with height away from the surface. These bad profiles generally occur when the naturally occurring variability is too large to be removed by our differencing technique. Examples of a good and bad profile are shown in Figure 4.

Our direct covariance measurements of the sensible heat, latent heat and momentum fluxes provide estimates of the scaling parameters, u_*, ρ_{v_*}, and L. The fluxes are corrected for platform motion (Edson et al., 1998). The scaling parameters are then combined with the measured

water vapor profiles to produce estimates of the dimensionless profile versus z/L shown in Figure 5.

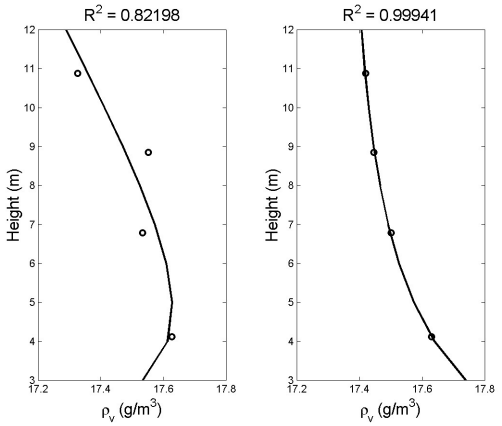

Figure 4: Representative examples of good (right) and bad (left) profiles used in our analysis based on R^2.

The two curves in Figure 5 are derived from two commonly used parameterizations for dimensionless water vapor profiles. These parameterizations are represented by

$$\phi_q\left(\frac{z}{L}\right) = \left(1 - a_q\frac{z}{L}\right)^{-N} \qquad (6)$$

where a_q and N are a numerical constant. The Businger-Dyer formula (Businger et al., 1971; Dyer, 1974) specify a value of approximately 16 for a_q and $1/2$ for N. In the convective limit, the dimensionless profiles are expected to become proportional to $(-z/L)^{-1/3}$ such that N is equal to $1/3$ (Carl et al., 1973). The TOGA-COARE bulk algorithm blends the two functional forms together such that $N = 1/2$ in near neutral conditions and $N = 1/3$ in (local) free convection (Fairall et al. 1996).

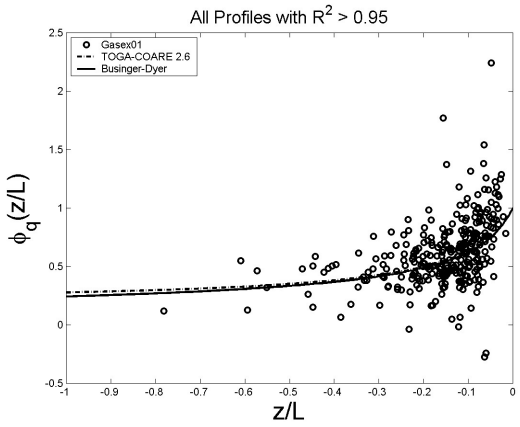

Figure 5: The dimensionless water vapor profile versus z/L. All points with $R^2 > 0.95$ are shown.

The least squares fit to the bin-averaged data is shown in Figure 6. These fits are plotted against the bin average of the data to give a clearer indication of the goodness of fit. The results for the two commonly used values of N are summarized in Table 1. The regression analysis shows that an exponent of ½ provides a better fit to the data in near neutral conditions, which agrees with the majority of previous investigations conducted over land.

Table 1. Numerical constants from regression analysis.

Exponent, N	a_q	R^2
1/2	14.3	0.87
1/3	44.3	0.75

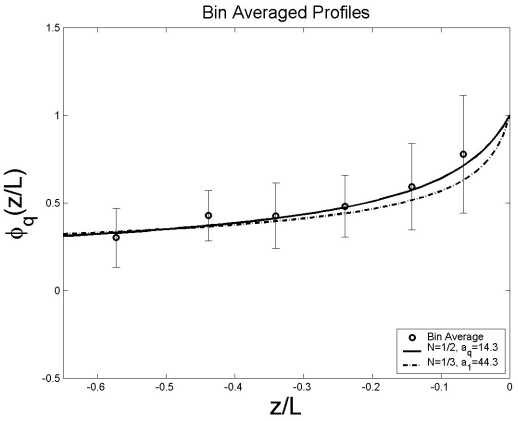

Figure 6: Bin-averaged values of the dimensionless water vapor profile. The error bars represent the standard deviation about the mean.

The profiles of water vapor can be used to compute ρ_{v_*} using the integral form of **(5)** given by

$$\overline{\rho_v}(z_1) = \overline{\rho_v}(z_2) + \frac{\rho_{v_*}}{\kappa}\left[\ln\left(\frac{z_1}{z_2}\right) - \psi_q\left(\frac{z_1}{L}\right) + \psi_q\left(\frac{z_2}{L}\right)\right] \qquad (7)$$

where

$$\psi_q(\zeta) = \int [1 - \phi_q(\zeta)]\frac{d\zeta}{\zeta} \qquad (8)$$

where $\zeta = z/L$. A linear fit of $\ln(z) - \psi_q(z/L)$ versus $\overline{\rho_v}(z)$ has a slope of κ/ρ_{v_*}. The latent heat flux can then be estimated by combining ρ_{v_*} with u_* as

$$Q_e = L_e u_* \rho_{v_*} \qquad (9)$$

where u_* can be derived from direct covariance, bulk aerodynamic, or profile estimates.

A comparison of the humidity scaling parameters derived from the profile and direct covariances methods are shown in Figure 7. The fluxes were computed from **(9)** using the direct covariance estimates of u_* and the profile estimate of ρ_{v_*}. The profile estimates used the integrated form of (6) given by Paulson (1970) with a_q = 14.3 and N = 1/2. Figure 7 shows that the flux estimates derived from the profile method are in good agreement with the fluxes derived from the direct covariance and bulk aerodynamic methods.

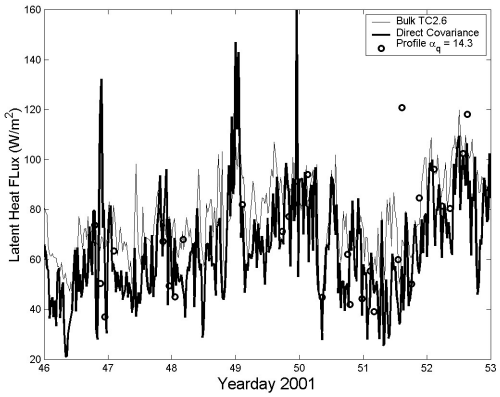

Figure 7: Time series of the latent heat flux estimates derived from the direct covariance, bulk aerodynamic and profile methods.

5. SUMMARY

Flux-profile relationships for water vapor were performed over the open ocean at 3°S an d 125°W. In this region, the atmospheric boundary layer was predominantly unstable and wind speeds ranged from 3-8 m/s. Profiles of water vapor, temperature, CO_2 and DMS were measured from a bow-mast system that extended 10 m from the bow of the NOAA R/V Ronald H. Brown. Profiles were measured 4-12 m from the ocean surface along with direct turbulent air-sea fluxes.

Results derived from the water vapor data show very good agreement with commonly used flux-profile relationships derived from overland measurements. This indicates that the MO similarity functions are applicable over the ocean in conditions where the theory is applicable, i.e., in surface layers where the structure of the turbulence is dominated by the relative importance of mechanical (i.e., wind shear) versus thermal forcing. In our preliminary analysis, values of a_q=14.3 and N=1/2 gives good agreement with our data.

The good agreement with previous investigations conducted overland indicates that the WBL has an indiscernible effect on the over water flux-profile relationships under these conditions. They also indicate that the differencing approach used in our analysis provides sufficiently accurate water vapor profiles. Application of this approach to other constituents such as biogenic and trace gases will allow us to investigate air-sea gas fluxes using the profile method with traditional flux-profile relationships.

ACKNOWLEDGMENTS

This research was supported by NSF grant OCE-9986724.

REFERENCES

Businger, J. A., J. C. Wyngaard, Y. Izumi and E. F. Bradley, 1971: Flux profile relationships in the atmospheric surface layer. *J. Atmos. Sci.*, **28**, 181-189.

Carl, M. D., T. C. Tarbell, H. A. Panofsky, 1973: Profiles of wind and temperature from towers over homogeneous terrain. *J. Atmos. Sci.*, **30**, 788-794.

Dyer, A. J., 1974: A review of flux-profile relations. *Bound.-Layer Meteor.*, **1**, 363-372.

Edson, J. B., A. A. Hinton, K. E. Prada, J. E. Hare, and C. W. Fairall, 1998: Direct covariance flux estimates from mobile platforms at sea. *J. Atmos. Oceanic Tech.*, **15**, 547-562.

Edson, J. B. and C. W. Fairall, 1998: Similarity relationships in the marine surface layer. *J. Atmos. Sci.*, **55**, 2311-2328.

Fairall, C. W., E. F. Bradley, D.P. Rogers, J. B. Edson, and G. S. Young, 1996: Bulk parameterization of air-sea fluxes for TOGA COARE. *J. Geophys. Res.,* **101**, 3747-3764.

McGillis, W.R., J. B. Edson, J. D. Ware, J. W. H. Dacey, J. E. Hare, C. W. Fairall, R. Wanninkhof. Carbon dioxide flux techniques performed during GasEx98. *J. Mar Chem.* **75**, 267-280, 2001.

Paulson, C. A., 1970: The mathematical representation of wind speed and temperature profiles in the unstable atmospheric surface layer. *J. Appl. Meteor.*, **9**, 857-861.